COMSOL CONFERENCE 2025 AMSTERDAM

A 2D Computational Model of a Packed-Bed Magnetic Refrigeration System

F. Rodríguez-Méndez[1], B. Chinè[1], M. Meneses-Guzman[2], F. Cugini[3], M. Solzi[3], S. Fabbrici[4], F. Albertini[4]

1. School of Materials Science and Engineering, Costa Rica Institute of Technology, Cartago, Costa Rica.
2. School of Industrial Production Engineering, Costa Rica Institute of Technology, Cartago, Costa Rica.
3. Department of Mathematical, Physical and Computer Sciences, University of Parma, Italy.
4. Institute of Materials for Electronics and Magnetism, National Research Council, Parma, Italy.

Abstract

In this work, a two-dimensional time-dependent model of a magnetic refrigeration system with an active magnetic regenerator (AMR) is developed to simulate a magnetocaloric device. The physical model consists of an AMR configured as a porous packed bed of spheres, two heat exchangers for the hot and cold environments, and a working fluid. The cyclic flow is described by the Brinkman equations for porous media, whereas the Local Thermal Nonequilibrium frame accounts for the heat transfer in the liquid, solid and porous domains. The coupling between these physics is added by using the COMSOL Multiphysics® Conjugate Heat Transfer option that combines the Heat Transfer in Solids and Fluids and the Porous Media Flow physics under the Non-Isothermal Flow Multiphysics interface. Then, the magnetocaloric effect is introduced by the inclusion of a source term in the energy equation that is dependent on the adiabatic temperature change and the specific heat of the magnetocaloric material. The latter two parameters are inserted into the model by using interpolated functions based on experimental magnetic behavior data for gadolinium, known for being the benchmark material for this application. Several time-dependent studies are carried out based on a Modern Design of Experiments (DOE) varying the working frequency, fluid velocity and the packed-bed porosity, aiming to optimize the device's response in terms of performance, cooling capacity and temperature span reached. The results yield that gadolinium offers moderate cooling capability and extended temperature span, but low COP (Coefficient of Performance).

Keywords: magnetocaloric materials, magnetic refrigeration, computational modeling and simulation, non-isothermal flow, uncertainty quantification.

1. Introduction

Refrigeration and air-conditioning systems account for roughly 17% of the global primary energy use [1] drawing almost 2000 TWh of electricity annually [2]. Moreover, most of these thermal management units rely on vapor-compression technology, which is responsible for about 7.8% of greenhouse-gas emissions [3]. Magnetic refrigeration, which employs a solid refrigerant, is widely regarded as a leading emerging alternative to vapor compression [4]. It can also have the potential to reach efficiencies up to 60% of the Carnot limit, along with a 20–30% reduction in energy consumption [5].

Magnetic refrigeration exploits the magnetocaloric effect (MCE): applying a magnetic field to a magnetocaloric material (MCM) alters its magnetic order and reduces its magnetic entropy. Under isentropic (adiabatic) conditions, total entropy is conserved, so the lattice entropy increases, producing an adiabatic temperature changeΔT_{ad} in the material [6].

Nowadays, there are several prototypes using the principle of magnetic refrigeration to obtain a competetive thermal span and cooling power [7]. However, significant work must be done not only in the field of materials science to obtain magnetocaloric materials with better properties [8], but also in the optimization of the working conditions and internal geometry of the system [9] .

Being the gadolinium (Gd) the benchmark material with the best reported properties [10], its adiabatic temperature change alone is not sufficient to achieve the temperatures required for most refrigeration applications – ΔT_{ad} of Gd at 1T magnetic field is only ~3K. To expand this operating range, an active magnetic regenerator (AMR) is used, i.e. a structure with an MCM in which a working fluid is pumped in the opposite direction to the heat flow. This regenerator has a double function, as it plays the role of both a cooling element and a heat regenerator.

Therefore, to generate a large temperature gradient, the operation of the AMR must ensure that the fluid keeps cycling from a cold end to a hot end of the device, taking the head load and transferring it to the environment [11]. A full cycle, with a Brayton-like approach [12], consists in four different steps: magnetization, hot flow, demagnetization, and cold flow.

There are different computational works modeling packed beds of gadolinium as AMR. Bouchard et al. [13] studied a regular matrix of Gd solid particles in

a water fluid and solved the coupled heat transfer and fluid flow equations of a transient three-dimensional model. Tagliafico et al. [14] developed a parametric analysis to evaluate the influence on the AMR performance of the operating frequency and fluid mass flow rate. Different configurations of porous regenerators have been studied in [15] using the same mass of Gd with the same AMR length and showing the best performance for the case of stacked parallel flat plates. Navickaite' et al. [16] proposed a novel flow structure of a solid active magnetic regenerator based on double corrugated tubes and compared it with conventional flows in porous media of packed spheres and in a cylindrical micro-channel matrix. Numerical investigations were carried out in [17] to analyze a porous regenerator with different particle diameters, utilization factors and operating frequencies, showing the influence of the viscous heating effect on the refrigeration capacity. Effatpisheh et al. [18] used a single layer of Gd for six-packed-sphere regenerators of a one-dimensional numerical model and conducted a parametric study to evaluate the performance of the system.

On the other hand, the usefulness of Design of Experiments (DoE) method in magnetic refrigeration was demonstrated by [19], who studied an AMR system consisting of stacked gadolinium plates. The authors applied a two-level 2^{7-3} fractional DoE based on Box methodology to evaluate the effect of seven parameters on the temperature span. The DoE was also applied to optimize the layer lengths of a 16-layer regenerator [20] carrying out 137 simulations with different MCM length distributions. Whereas Aprea et al. [21] used artificial neural networks to develop a control technique to maximize the working of a rotary permanent magnetic refrigerator. Other statistical techniques have been applied by Silva et al. [22] to dimension any type of magnetocaloric system by training learning classifiers. Also, the same authors in [23], applied a machine learning method to predict three performance values of magnetocaloric heat pumps, such as temperature span, heating power and COP (Coefficient of Performance). Gaussian process regression has been used by [24] to find statistical correlations and predict the relative cooling power of magnetic refrigeration devices when using ferromagnetic lanthanum manganites as magnetocaloric materials.

In this work we use COMSOL Multiphysics® 6.2 to develop a two-dimensional time-dependent model of a magnetic refrigeration system with an active magnetic regenerator (AMR), simulating a magnetocaloric device. The physical model consists of an AMR configured as a porous packed bed of spheres, two heat exchangers for the hot and cold environments, and a working fluid. ΔT_{ad} and heat capacity of the material are measured experimentally rather than mean field approximations, and the fluid motion considers viscous losses. Main metrics used to evaluate the magnetic device performance are the maximum temperature span obtained, the cooling capacity at no-load condition, and the coefficient of performance (COP). The study takes into consideration free and porous media flow and conjugated heat transfer mechanisms in the system. Then, an uncertainty quantification study is carried out to identify the most influential input parameters for the AMR temperature span.

The structure of the paper is the following. The description of the physical model and the governing equations are given in Section 2. The computational results, including the uncertainty quantification studies, are presented and discussed in Section 3. Finally, Section 4 summarizes the main conclusions of the work.

2. Model of the AMR System

2.1. Physical model

In the system depicted in Fig. 1, the packed-bed magnetic regenerator is made of Gd, the cold and hot heat exchangers are built of copper, and the heat transfer fluid is pure water. The model is based on the COMSOL Multiphysics® Heat Transfer Module [25] and CFD Module [26], coupling the Heat Transfer in Solids and Fluids with the Free and Porous Media Flow physics under the Non-Isothermal Flow Multiphysics interface. The dependent variables, such as fluid pressure and velocity, and temperature distribution across the AMR, are solved using the Finite Element Method. The velocity and pressure profiles are first determined along the fluid and then they are used to solve the temperature distribution in both the solid and fluid domains during the cold and hot fluid flows, respectively. This process is repeated for several cooling cycles for the system to reach a steady-state condition.

The geometrical configuration implemented in the model is summarized in Table 1. For a Brayton refrigeration cycle, the time steps for the four stages are symmetrically distributed. This parameter, along with others of equal importance, such as the strength of the magnetic field, the cycle period, the fluid velocity in the fluid flows phases, packed-bed porosity, sphere diameter, permeability, and the heat transfer coefficients for the outward boundaries of the heat exchangers are provided in Table 2.

Table 1. *Geometrical configuration of the AMR system.*

Part	Dimensions in mm
Regenerator	80 x 10
Cold heat exchanger	50 x 10
Hot heat exchanger	50 x 10
Fluid channel	230 x 10
Heat exchanger-regenerator gap	10

Table 2. Initial and working conditions of the AMR model.

Parameter	Value
Magnetic field strength	1.8T
Total cycle period	2s
Frequency	0.5 s^{-1}
Fluid flows step time	1s
(de)magnetization step time	1s
Displaced fluid volume	15%
Maximum fluid velocity at inlet	0.024 m/s
Convective heat transfer coefficient at CHEX (h_C)	0 W/(m^2.K)
Convective heat transfer coefficient at HHEX (h_H)	10E^3 W/(m^2.K)
Initial value of temperature	292K
Sphere cell diameter	0.5 mm
Porosity ε_p	0.350
Permeability	1.69E^{-10}m^2

2.2. Governing equations

Assuming the fluid flow is laminar, the velocity distribution in the fluid domain is determined by solving the Navier-Stokes momentum and continuity equations

$$\rho\left(\frac{\partial \boldsymbol{u}}{\partial t} + (\boldsymbol{u}\cdot\nabla)\boldsymbol{u}\right) = \nabla\cdot[-p\,\mathbf{I} + \mu[\nabla\mathbf{u} + \{\nabla\mathbf{u}\}^{\mathrm{T}}] + \mathbf{F} \quad (1)$$

$$\rho\nabla\cdot\boldsymbol{u} = 0 \quad (2)$$

where ρ is the density (kg/m^3), $\mathbf{u}$ (m/s) is the velocity in a fluid domain, p (Pa) is the pressure, μ is the viscosity (Pa·s), $\mathbf{I}$ mean the identity tensor, $\mathbf{F}$ are the volume external forces applied to the fluid (N/m^3), and t is time.

Then, for the porous region, we use the Brinkman equations to compute fluid velocity and pressure fields under laminar flow regime, which includes a term in the momentum balance for the viscous transport. If ε_p is the porosity, κ (m^2) the permeability, and Q_m (kg/(m^3·s) a mass source or sink, the conservation of the linear momentum is

$$\frac{\rho}{\varepsilon_p}\frac{\partial \boldsymbol{u}}{\partial t} + \frac{\rho}{\varepsilon_p}(\boldsymbol{u}\bullet\nabla) = -\nabla p + \nabla\bullet\left[\frac{1}{\varepsilon_p}\left\{\mu(\nabla\boldsymbol{u} + (\nabla\boldsymbol{u})^T - \frac{2\mu}{3}(\nabla\bullet\boldsymbol{u})\boldsymbol{I}\right\}\right] - \left[\kappa^{-1}\mu + \rho\beta|\mathbf{u}| + \frac{Q_m}{\varepsilon_p{}^2}\right]\mathbf{u} + \mathbf{F} \quad (3)$$

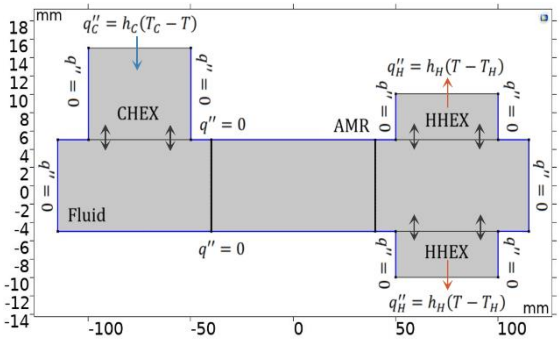

Figure 1. AMR model and boundary conditions used.

where the magnitude $-\rho\beta|\mathbf{u}|\mathbf{u}$ represents the viscous Forchheimer drag force, and β is a parameter dependant on the porous medium permeability.

Next, or the solid copper region of the heat exchangers, in absence of heat sources, the conservation of the thermal energy is represented by the following Fourier equation

$$\rho_s c_{p,s}\frac{\partial T_s}{\partial t} - k_s\nabla^2 T_s = \dot{Q}_{HT} \quad (4)$$

where $c_{p,s}$ is the specific heat capacity of the solid, T_s is the solid temperature, and k_s is the constant solid thermal conductivity. For the water fluid region, the conservation of the thermal energy is

$$\rho\, c_{p,f}\left(\frac{\partial T_f}{\partial t} + (\boldsymbol{u}\cdot\nabla)T_f\right) - k_f\nabla^2 T_f = -\dot{Q}_{HT} \quad (5)$$

where $c_{p,f}$ is the fluid specific heat, T_f is the fluid temperature, and k_f is the fluid thermal conductivity. In both equations (4) and (5) the $\dot{Q}_{HT}$ term is the heat transferred through the solid-liquid interface.

Whereas in the porous AMR, because of the magnetization-demagnetization cycle and the fluid flow, the temperature of the solid domain of the regenerator T_s is different to the temperature of the working fluid T_f. This means that there is no thermal equilibrium between the solid and fluid domains. For this reason, an additional source term quantifying the exchanged heat between both phases is needed, therefore, we have the following conservation energy

$$(1-\varepsilon_p)\rho_s C_{p,s}\frac{\partial T_s}{\partial t} + \nabla\cdot\boldsymbol{q}_s = q_{s,f}(T_f - T_s) + (1-\varepsilon_p)\dot{Q}_{MCE} \quad (6)$$

$$\varepsilon_p\rho_f C_{p,f}\frac{\partial T_f}{\partial t} + \varepsilon_p\rho_f C_{p,f}\boldsymbol{u_f}\cdot\nabla T_f + \nabla\cdot\boldsymbol{q}_f = q_{s,f}(T_s - T_f) \quad (7)$$

with $\boldsymbol{q}_s$ and $\boldsymbol{q}_f$ are the solid and fluid conductive heat fluxes, respectively.

Concerning the MCE, this is introduced in the term $\dot{Q}_{MCE}$ as a heat source in the equation (6) and defined as a function of $\Delta T_{ad}(H,T)$ and $c_p(H,T)$ of the MCM. Is it important to note that both factors are dependent on the applied magnetic field and the instant temperature of the regenerator. The relation that describes this effect is modeled by

$$\rho_s c_p(H,T)\frac{\Delta T_{ad}(H,T)}{dt} = \dot{Q}_{MCE} \quad (10)$$

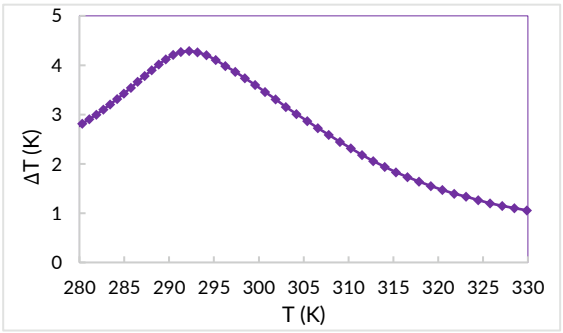

Figure 2. ΔT_{ad} for Gd under a magnetic field of 1.8T.

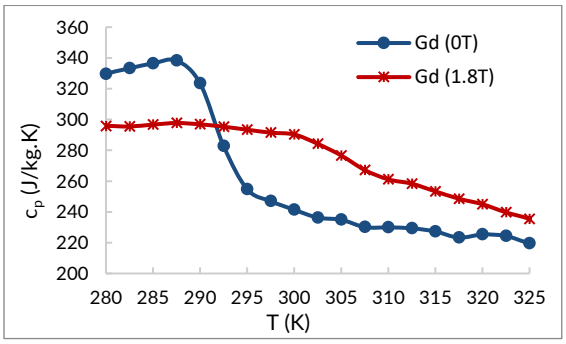

Figure 3. *Specific heat values for Gd under a magnetic field of 0T and 1.8T.*

$\Delta T_{ad}(H,T)$ and $c_p(H,T)$ parameters are introduced in the model by using interpolated functions based on experimental data for the Gd, as illustrated in Figs. 2 and 3.

2.3. Boundary conditions

A water flow is set at the inlet of the system as a reciprocating piston flow with a maximum velocity of 0.024 m/s, whereas at the outlet a relative pressure equal to zero is imposed. Also, no-slip conditions are used on the solid walls.

As shown in Fig. 1, the external boundaries are adiabatic, except for the outward boundaries of CHEX and HHEX, which have a prescribed heat flux. The solid domains and the fluid are assumed to be in perfect contact following the boundary condition

$$\left(k_f \frac{\partial T_f}{\partial y}\right)\Big|_{y=H_{fl}} = \left(k_s \frac{\partial T_s}{\partial y}\right)\Big|_{y=H_{fl}} \quad (11)$$

For the latter parameter, perfect thermal contact between the hot heat exchanger and the outside environment is assumed by making the value of the heat transfer coefficient in the outward boundary of the hot end very large. On the other hand, to assess the performance of the regenerator at maximum cooling capacity, the heat transfer coefficient at the CHEX is set to 0 W/(m^2.K).

2.4. Performance evaluation metrics

The assessment of the performance of the system is determined by the temperature span achieved for the device, its cooling capacity, and COP. ΔT_{span} is the temperature difference between the hot and cold heat exchangers. The cooling capacity is calculated by the amount of cooling per cycle absorbed for the CHEX

$$q_c' = \int_0^{\tau}\int_0^{L_{HEX}} \dot{q_c''}\, dxdt \quad (12)$$

where τ is the cycle period and L_{HEX} is the length of the heat exchanger. For the system COP, we need to calculate the rejected heat per cycle in the HHEX as

$$q_r' = \int_0^{\tau}\int_0^{L_{HEX}} \dot{q_r''}\, dxdt \quad (13)$$

Then, the total work (w_{tot}') done by the AMR is the sum of the work required to magnetize the regenerator, and the work required to displace the fluid. The first term is described by the equation

$$w_{mag}' = q_r' + q_c' \quad (14)$$

meanwhile the pumping power required to move the working fluid through the AMR can be solved by the relationship

$$\dot{w}_{pump} = \frac{U_f \nabla p}{\eta_{pump}} \quad (15)$$

where η_{pump} is the pump efficiency, assumed to be around 0.8 for most commercial devices.

Then, the COP of the refrigerator is calculated by

$$COP = -\frac{q_c'}{w_{tot}'} \quad (16)$$

3. Simulation Results and Discussion

3.1. MCMs assessment

Fig. 4 shows the development of the ΔT in time for the Gd material in the AMR (both ends of the regenerator). The simulation was performed over 600 cycles with a period of 2s, which is equivalent to a global time of 1200s. As expected, the Gd is capable of build a quite larger AMR ΔT, due to its ΔT_{ad}. It is also noticeable that, for the total cycles simulated, the Gd doesn't arrive to a steady-state regime, where the ΔT between two consecutive cycles is equal or less than 0.01K, meaning that it would be necessary to increase the final time to fulfill this condition.

Figs. 5 shows the 2D temperature evolution across the entire magnetic device during the cold blow stage of the Brayton cycle. In the cold blow step of the cooling cycle, the heat generated in the AMR due to the MCE is transferred into the working fluid and moved towards the HHEX, where it will heat up the hot side of the system. On the other way around, during the hot blow phase, after the regenerator is demagnetized, the temperature of the fluid is lowered by the colder AMR. Then, the cooled fluid is transferred towards the CHEX, reducing the temperature of the cold side of the system.

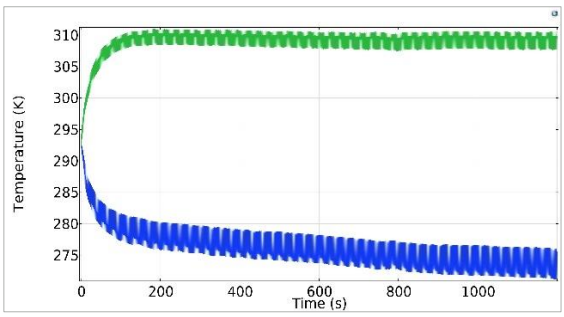

Figure 4. *ΔT behavior over time at the hot and cold ends of the porous AMR.*

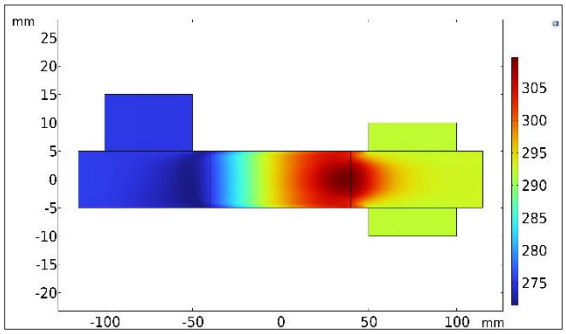

Figure 5. *Temperature gradient across the porous AMR during the cold blow stage.*

3.2. Performance Evaluation

Three metrics are used to evaluate the MCM studied in the simulations: first, the ΔT_{span} between the cold and hot heat exchangers of the system; and second and third, the cooling power and the coefficient of performance (COP) at no-load.

For the latter two parameters, as stated in Eq. 15, pressure losses along the AMR and the fluid velocity are needed. Pressure losses are ~34.45kPa between the ends of the regenerator and are a consequence of the porous geometry of the AMR. The average velocity obtained during the hot and cold flows was 0.025m/s. Table 3 summarizes the results for the performance metrics of the system. These values indicate that the AMR can sustain a substantial cooling load at a moderate temperature span, while operating with moderate efficiency. The kW-level cooling capacity highlights effective regeneration and strong heat exchange between the fluid and the porous matrix, while the temperature span demonstrates the ability of the device to create a usable gradient near room temperature. The COP value, although modest compared to most air conditioners, for example, is consistent with expected losses in most AMRs, due to low working frequencies, pressure drop, and non-ideal temperature distribution.

Table 3. *Performance parameters of the system.*

Parameter	Value
Temperature span	16.83K
Cooling capacity	1274.69W
Coefficient of performance	1.41

3.3. Uncertainty Quantification

The AMR performance metrics analyzed depend on many parameters, therefore a full numerical Design of Experiments (DoE) study would be prohibitive, because it will demand a very high computational time. To reduce the complexity of the analysis, we assume some uncertainty in only three parameters of the AMR system, identified as fundamental in the literature, namely working frequency (*w_freq*) and displaced fluid volume (*V_disp*), both controlling the fluid velocity, and packed-bed porosity (*por*). Also, we select the temperature span as the quantity of interest (QoI), since it is one of the most representative metric of performance.

Here, the temperature span selected for the incoming analysis was measured as the difference between the AMR regenerator ends, yielding ~37.5K after the simulated time of 1200s. Thus, we carry out Uncertainty Quantification (UQ) studies to compute the resulting probability distributions for the temperature span to be lower than this threshold value.

The parameters that participate in the UF quantification are all assumed to be normally distributed around their nominal values according to Table 4, which also gives the values of the standard deviation and the cumulative distribution function levels, both for the lower bound (CDF-lower) and the upper bound (CDF-upper). For all the parameters, the standard deviation is equal to 1% of the mean value, additionally, the cumulative distribution levels are selected following the same approach.

Table 4. *Input-parameter distributions used in the uncertainty quantification analysis.*

Parameter	Magnitude	Value
Frequency	Mean (*w_freq*)	0.5 s^{-1}
	Standard deviation	0.01x *w_freq*
	CDF-lower	0.95* *w_freq*
	CDF-upper	1.05* *w_freq*
Displaced fluid volume	Mean (*V_disp*)	15%
	Standard deviation	0.01x *V_disp*
	CDF-lower	0.95* *V_disp*
	CDF-upper	1.05* *V_disp*
Porosity	Mean (*por*)	0.350
	Standard deviation	0.01x *por*
	CDF-lower	0.95* *por*
	CDF-upper	1.05* *por*

Then, using the UQ Module in Comsol Multiphysics [27], we develop four different study types:

a) screening, to identify the most influential input parameters for the AMR temperature span (*AMR_DT*), based on the Morris One-At-a-Time (MOAT) method;
b) sensitivity analysis, to compute the fraction of impact for the inputs for the *AMR_DT*, using first order and total Sobol indices;
c) uncertainty propagation, to evaluate the statistical variation of the *AMR_DT* by a kernel density estimation (KDE) plot, representing an estimate of its probability distribution;
d) reliability analysis, to calculate the probability for the condition where *AMR_DT* is lower than 37.5K.

The UQ study needs to get statistical data based on the computational model, then, to reduce the number of simulations, we built in Comsol Multiphysics a so-called surrogate model that is used for sensitivity study, uncertainty propagation, and reliability analysis. In our work, we have selected a surrogate model based on the Gaussian Process.

For the screening study, Fig. 6 gives a MOAT plot indicating that the displaced fluid volume is the most influential parameter for the AMR temperature span, followed by the frequency. However, the porosity also appears to be significant. Indeed, a high value of the MOAT mean value indicates that the parameter is significantly influencing the quantity of interest, but a high value of the MOAT standard deviation means that the parameter is influential and that it is either interacting with other parameters, and/or that it has a nonlinear influence. The results of the sensitivity analysis based on the Sobol method, also known as variance-based sensitivity analysis, have confirmed the former findings.

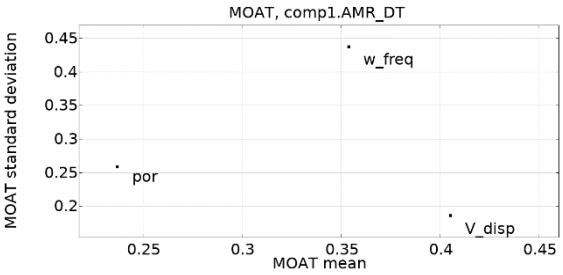

Figure 6. *MOAT plot from screening study, indicating general effect on x-axis and nonlinearity on y-axis.*

Then, the probability density function of the AMR temperature span, evaluated in the uncertainty propagation step, has provided information about the joint effect of the uncertainties in all varied parameters, which was resumed graphically in a KDE plot. Finally, the risk for the AMR temperature span to be lower than the settled threshold values of 37.5K has been computed with the reliability analysis, giving a probability of about 3 %.

4. Conclusions

In this study, we built and validated a 2-dimensional, time-dependent AMR model of a packed bed with gadolinium spheres that couples Brinkman porous flow with local thermal nonequilibrium heat transfer and an experimentally based MCE source term, and we used it to quantify device-level performance and parameter sensitivities under a 1.8 T, 2s Brayton-like cycle. The simulations delivered a temperature span across the heat exchangers of 16.83K, a cooling capacity of 1274.69W, and COP = 1.41 at no-load, with a computed pressure drop of ~34.45kPa and mean blow velocity near 0.025m/s, values consistent with a reliable regeneration but noticeable hydraulic losses. An uncertainty-aware exploration (frequency, displaced fluid volume, and packed bed porosity) shows displaced volume and frequency as the most influential parameters, but with a non-negligible porosity contribution. Additionally, the UQ studies indicate a modest risk (~3%) of failing a 37.5 K regenerator-end temperature span threshold used for internal diagnostics.

Acknowledgements

The first three authors gratefully acknowledge the financial aid provided by the Vicerrectoría de Investigación y Extensión of the Instituto Tecnológico de Costa Rica, through the project 1490040 "*Materiales Magnetocalóricos para Aplicaciones de Refrigeración Magnética y Recolección de Energía Térmica*". F. Rodriguez-Mendez gratefully acknowledges the support provided by the Postgraduate Office of the Instituto Tecnológico de Costa Rica. S. Fabbrici and F. Albertini acknowledge financial support from PNRR MUR project ECS_00000033_ECOSISTER.

References

[1] C. Aprea, A. Greco, A. Maiorino and C. Masselli, "Analyzing the energetic performances of AMR regenerator working with different magnetocaloric materials: Investigations and viewpoints," *International Journal of Heat and Technology,* vol. 35, no. 1, pp. S383-S390, 2017.

[2] International Energy Agency, "The Future of Cooling," 2018. [Online]. Available: http://www.iea.org/reports/the-future-of-cooling. [Accessed July 2023].

[3] D. Coulomb, J.-L. Dupont and V. Morlet, "The Impact of the Refrigeration Sector on Climate Change," 35th Informatory Note on Refrigeration Technologies, Technical Report, International Institute of Refrigeration, Paris, France, 2016.

[4] A. Kitanovski, U. Plaznik, U. Tomc and A. Poredos, "Present and future caloric refrigeration and heatpump technologies," *International Journal of Refrigeration,* vol. 57, pp. 288-298, 2015.

[5] E. Brück, O. Tegus, D. Thanh and K. Buschow, "Magnetocaloric refrigeration near room temperature," *Journal of Magnetism and Magnetic Materials,* vol. 310, no. 2, pp. 2793-2799, 2007.

[6] S. Choi, U. Han, H. Cho and H. Lee, "Review: Recent advances in household refrigerator cycle technologies," *Applied Thermal Engineering,* no. 132, pp. 560-574, 2018.

[7] A. Greco, C. Aprea, A. Maiorino and C. Masselli, "A review of the state of the art of solid-state caloric cooling processes at room-temperature before 2019," *International Journal of Refrigeration,* vol. 106, p. 66–88, 2019.

[8] T. Gottschall, K. P. Skokov, M. Fries, A. Taubel, I. Radulov, F. Scheibel, D. Benke, S. Riegg and O. Gutfleisch, "Making a Cool Choice: The Materials Library of Magnetic Refrigeration," *Advanced Energy Materials,* vol. 9, no. 34, 2019.

[9] A. Kitanovski, "Energy Applications of Magnetocaloric Materials," *Advanced Energy Materials,* vol. 10, no. 10, 2020.

[10] M. Balli, O. Sari, C. Mahmed, C. Besson, P. Bonhote, D. Duc and J. Forchelet, "A pre-industrial magnetic cooling system for room temperature application," *Applied Energy,* vol. 98, pp. 556-561, 2012.

[11] H. Ucar, D. Paudyal and O. Boyraz, "Using numerical methods to screen magnetocaloric materials in an active magnetic regenerative cycle," *International Journal of Refrigeration,* vol. 120, pp. 50-57, 2020.

[12] J. Tusek, A. Kitanovski, S. Zupan, I. Prebil and A. Poredos, "A comprehensive experimental analysis of gadolinium active magnetic regenerators," *Applied Thermal Engineering,* vol. 53, pp. 57-66, 2013.

[13] J. Bouchard, H. Nesreddine and N. Galanis, "Model of a porous regenerator used for magnetic refrigeration at room temperature," *International Journal of Mass and Heat Transfer,* vol. 52, pp. 1223-1229, 2009.

[14] G. Tagliafico, F. Scarpa and L. A. Tagliafico, "Dynamic 1D Model of an Active Magnetic Regenerator: A Parametric Investigation," *Journal of Mechanical Engineering,* vol. 58, pp. 9-15, 2012.

[15] D. Vuarnoz and T. Kawanami, "Numerical Analysis of Different Active Magnetic Regenerator (AMR) Configurations," in *13th International Conference on Sustainable Energy technologies (SET2014)*, Geneva, 2014.

[16] K. Navickaite, C. Bahl and K. Engelbrecht, "Nature-Inspired Flow Patterns for Active Magnetic Regenerators Assessed Using a 1D AMR Model," *Frontiers in Energy Research,* vol. 7, no. 68, 2019.

[17] H. Shi, T. Ma and Q. Wang, "Numerical Investigations of a Packed-Bed Active Magnetic Regenerator," *Chemical Engineering Transactions,* vol. 70, pp. 739-744, 2018.

[18] A. Effatpisheh, A. Vadiee and B. Monfarred, "Mathematical Modelling of Active Magnetic Regenerator Refrigeration System for Design Considerations," *Energies,* vol. 13, p. 6301, 2020.

[19] J. Rodaut, H. Bouchekara, A. Kedous-Lebouc and J. Coulomb, "Optimization of active magnetic regenerative refrigeration systems using design of experiments," in *The 3rd International Conference of IIR on Magnetic Refrigeration at Room Temperature*, Des Moines, USA, 2009.

[20] M. Zhang, O. Abdelaziz, A. M. Momen and A. Abu-Heiba, "A numerical analysis of a magnetocaloric refrigerator with a 16-layer regenerator," *Scientific Reports,* vol. 7, 2017.

[21] C. Aprea, A. Greco and A. Maiorino, "An application of the artificial neural network to optimise the energy performances of a magnetic refrigerator," *International Journal of Refrigeration,* vol. 82, pp. 238-251, 2017.

[22] D. Silva, J. Amaral and V. Amaral, "Broad Multi-Parameter Dimensioning of Magnetocaloric Systems Using Statistical Learning Classifiers," *Frontiers in Energy Research,* 2020.

[23] D. Silva, J. Ventura and J. Araujo, "Predicting the performance of magnetocaloric systems using machine learning regressors," *Energy and AI,* vol. 2, 2020.

[24] Y. Zhang and X. Xu, "Relative cooling power modeling of lanthanum manganites usin Gaussian process regression," *RCS Advances,* vol. 10, pp. 20646-20653, 2020.

[25] Comsol-Multiphysics, "Heat Transfer Module v6.2- User's Guide," 2023.

[26] Comsol-Multiphysics, "CFD Module v6.2-User's Guide," 2023.

[27] Comsol-Multiphysics, "Uncertainty Quantification Module v6.2-User's Guide," 2023.